SCIENCE CHINA
Earth Sciences

•RESEARCH PAPER•

July 2018 Vol.61 No.7: 925–939
https://doi.org/10.1007/s11430-017-9168-9

Distribution of glycerol dialkyl glycerol tetraethers in surface soils along an altitudinal transect at cold and humid Mountain Changbai: Implications for the reconstruction of paleoaltimetry and paleoclimate

Yue LI[1], Shijin ZHAO[1], Hongye PEI[1], Shi QIAN[1], Jingjie ZANG[1], Xinyue DANG[1] & Huan YANG[1,2*]

[1] *School of Earth Sciences, China University of Geosciences, Wuhan 430074, China;*
[2] *State Key Laboratory of Biogeology and Environmental Geology, China University of Geosciences, Wuhan 430074, China*

Received August 7, 2017; revised November 15, 2017; accepted March 1, 2018; published online April 12, 2018

Abstract Glycerol Dialkyl Glycerol Tetraethers (GDGTs) serve as important tools for the quantitative reconstruction of paleoclimate and paleoecology in both continental and marine environments. Previous studies of GDGTs in the terrestrial environments focused primarily on the soils from the relatively warm-humid or cold-dry regions. However, it is still unclear how GDGTs respond to environmental variables in the cold-humid regions. Here, we collected soils along an altitudinal transect of Mountain (Mt.) Changbai, which has a typical cold-humid climate, to investigate the distribution of GDGTs and the response of GDGT-based proxies to changes in climate along the transect. The shift in the distribution of archaeal isoprenoidal GDGTs (isoGDGTs) revealed that the archaeal community varied significantly along the transect, which can affect the relationship between TEX_{86} and mean annual air temperature (MAT). In addition, the increased temperature seasonality at higher altitudes exerted a significant impact on TEX_{86}. We proposed a global calibration of TEX_{86} for the growing season temperature reconstruction in the soil environments: T=85.19×TEX_{86}− 46.30 (R^2=0.84, p<0.001). The methylation indices for 5-methyl branched GDGTs (brGDGTs) including MBT'_{5me} and $MBT_{5/6}$, showed correlation with soil water content but no relationship with MAT, indicating that $MBT'_{5me}$and $MBT_{5/6}$ from cold-humid environments may be not suitable for temperature and altitude reconstruction. In contrast, the recently developed pH proxies, including MBT'_{6me} (the methylation index for 6-methyl brGDGTs), CBT (Cyclisation index of Branched Tetraethers), $IR_{IIa'}$ (Isomer ratio of IIa′) and $IR_{IIIa'}$ (Isomer ratio of IIIa′) exhibited significant correlations with soil pH, suggesting these proxies can still be used for soil pH reconstruction in the cold-humid regions. The combination of MBT'_{5me} and MBT'_{6me} was strongly related to different types of climate (cold-dry, warm-humid, cold-humid, and warm-dry). For example, MBT'_{5me}<0.65 and MBT'_{6me}>0.55 are diagnostic for the cold-humid climate. Thus, the combination of MBT'_{5me} and MBT'_{6me} has the potential as a tool for the identification of different types of paleoclimate.

Keywords Cold-humid climate, GDGTs, Temperature, Soil pH, Soil water content

Citation: Li Y, Zhao S J, Pei H Y, Qian S, Zang J J, Dang X Y, Yang H. 2018. Distribution of glycerol dialkyl glycerol tetraethers in surface soils along an altitudinal transect at cold and humid Mountain Changbai: Implications for the reconstruction of paleoaltimetry and paleoclimate. Science China Earth Sciences, 61: 925–939, https://doi.org/10.1007/s11430-017-9168-9

* Corresponding author (email: yhsailing@163.com)

1. Introduction

The reconstruction of paleoaltimetry is an important approach to understanding the plateau uplift and regional tectonic movement. Recently, a number of proxies have been developed for the reconstruction of paleoaltimetry. They can be divided into three groups according to the principles that they are based upon: (1) Hydrogen and oxygen isotopic composition, e.g. δD of *n*-alkanes from the plant leaf waxes. Significant hydrogen and oxygen isotopic fractionation occurs when the water vapor ascends with the altitude. Proxies can be developed according to the relationship between altitude and the fractionation of hydrogen and oxygen isotopes (Jia et al., 2008; Zhuang et al., 2014; Bai et al., 2015). Water with different oxygen isotopic compositions can be ingested by animals and thus δ^{18}O of the mammal teeth can be used to reconstruct paleoaltimetry (Bershaw et al., 2010). (2) Temperature generally decreases with altitude, and paleothermometers, e.g. Δ47 of the carbonate (Ghosh et al., 2006; Hough et al., 2014), and TEX_{86} (tetraether index of archaea) (Liu et al., 2013; Yang et al., 2010, 2016), can be used to reconstruct the paleoaltimetry when the lapse rate is determined. (3) The assemblages of animal and plant fossils, e.g. mammalian skeleton fossils (Deng et al., 2011) and pollens (Sun et al., 2014). Plants and animals living in a specific niche can be used to constrain the environmental conditions including temperature, precipitation and altitude. However, each proxy has its strengths and weakness. It is necessary to deepen our understanding of the mechanisms of these proxies via further modern observations.

Glycerol dialkyl glycerol tetraethers (GDGTs) are a suite of lipids widely used in the reconstruction of paleotemperature (Schouten et al., 2013). Based on this, they were also thought to be potentially useful in the paleoaltimetry reconstruction (Ding et al., 2015; Yang et al., 2016). They can be divided into two groups: archaeal isoprenoidal GDGTs (isoGDGTs) and bacterial branched GDGTs (brGDGTs) (Figure 1). Thaumarchaeota can produce a diagnostic isoGDGT containing a cyclohexyl ring (Schouten et al., 2013). The relative number of cyclopentyl rings in the Thaumarchaeotal isoGDGTs are strongly correlated with the sea surface temperature (SST), and TEX_{86} (tetraether index of tetraethers consisting of 86 carbon atoms) was proposed to be a proxy for the SST estimation (Schouten et al., 2002, 2013; Zhou et al., 2014). Kim et al. (2010) later proposed two proxies, TEX_{86}^{H} and TEX_{86}^{L}, for the SST reconstruction in the high and low temperature marine environments, respectively. The application of TEX_{86} has been extended to the lake environments (Blaga et al., 2008, 2011; Powers et al, 2004, 2010). However, due to the complexity of archaeal community in the lakes and the impact of terrigenous archaeal isoGDGTs, the use of TEX_{86} for the lake surface temperature estimation has been only limited to the deep lakes with large catchment areas (Powers et al., 2010). In the terrestrial environments, e.g. soils and karst caves, TEX_{86} in the soils and stalagmites were demonstrated to be strongly related to temperature, but the calibration equations for them were different from those for the marine and lake environments (Liu et al., 2013; Blyth and Schouten, 2013; Blyth et al., 2014; Yang et al., 2016). TEX_{86} has been also suggested to reflect temperatures of different altitudes at mountains with different climates, and the calibration of TEX_{86} for temperature estimation was also different among studies (Yang et al., 2010, 2016; Liu et al., 2013).

BrGDGTs, which differ from isoGDGTs in the alkyl chains, were presumed to be produced by unknown anaerobic heterotrophic bacteria (Weijers et al., 2006, 2010; Oppermann et al., 2010). Weijers et al. (2007) found that CBT (the cyclization ratio of branched tetraethers), expressing the relative amount of cyclopentyl moieties in brGDGTs, strongly correlated with soil pH whereas MBT (the methylation index of branched tetraethers), reflecting the relative number of methyls in brGDGTs, were significantly related to soil pH and mean annual air temperature (MAT). Peterse et al. (2012) modified the original MBT proxy, and proposed a global calibration of MBT′/CBT for the MAT reconstruction. In the arid and semi-arid region of China, MBT′/CBT showed a strong dependence on soil moisture and precipitation (Wang et al., 2014; Yang et al., 2014a). The applicability of MBT (MBT′)/CBT as a temperature proxy has been tested in a multitude of altitudinal transects across the globe, including Mt. Kilimanjaro in Tanzania (Sinninghe Damsté et al., 2008), Mt. Gongga (Peterse et al., 2009), Mt. Xiangpi (Liu et al., 2013), Mt. Jianfengling (Yang et al., 2010), Mt. Shennongjia (Yang et al., 2016), the southeastern margin of the Tibetan Plateau (Deng et al., 2016), southern Alps (Zhuang et al., 2015), Mt. Meghalaya in India (Ernst et al., 2013), Mt. Rungwe in Tanzania (Coffinet et al., 2014), and eastern Cordillera in Colombia (Anderson et al., 2014). The linear relationship between temperature and altitude makes it possible to use MBT (MBT′)/CBT for the reconstruction of paleoaltimetry.

Recently, the improved chromatography methodology provides a way to further understanding the mechanism of the MBT (MBT′)/CBT proxy. De Jonge et al. (2013) found that GDGT-II and -III had isomers that have different methyl positions, namely, 5- and 6-methyl brGDGTs. The methylation index of 5-methyl brGDGTs (MBT'_{5me}) and 6-methyl GDGTs (MBT'_{6me}) were found to be dependent on temperature and soil pH, respectively, in the global soils (De Jonge et al., 2014a). The calculation of original MBT(MBT′) involves 5- and 6-methyl brGDGTs, which can essentially explain the dependence of MBT(MBT′) on both MAT and soil pH. After precluding 6-methyl brGDGTs, MBT'_{5me} can produce more accurate MAT than MBT′/CBT (De Jonge et

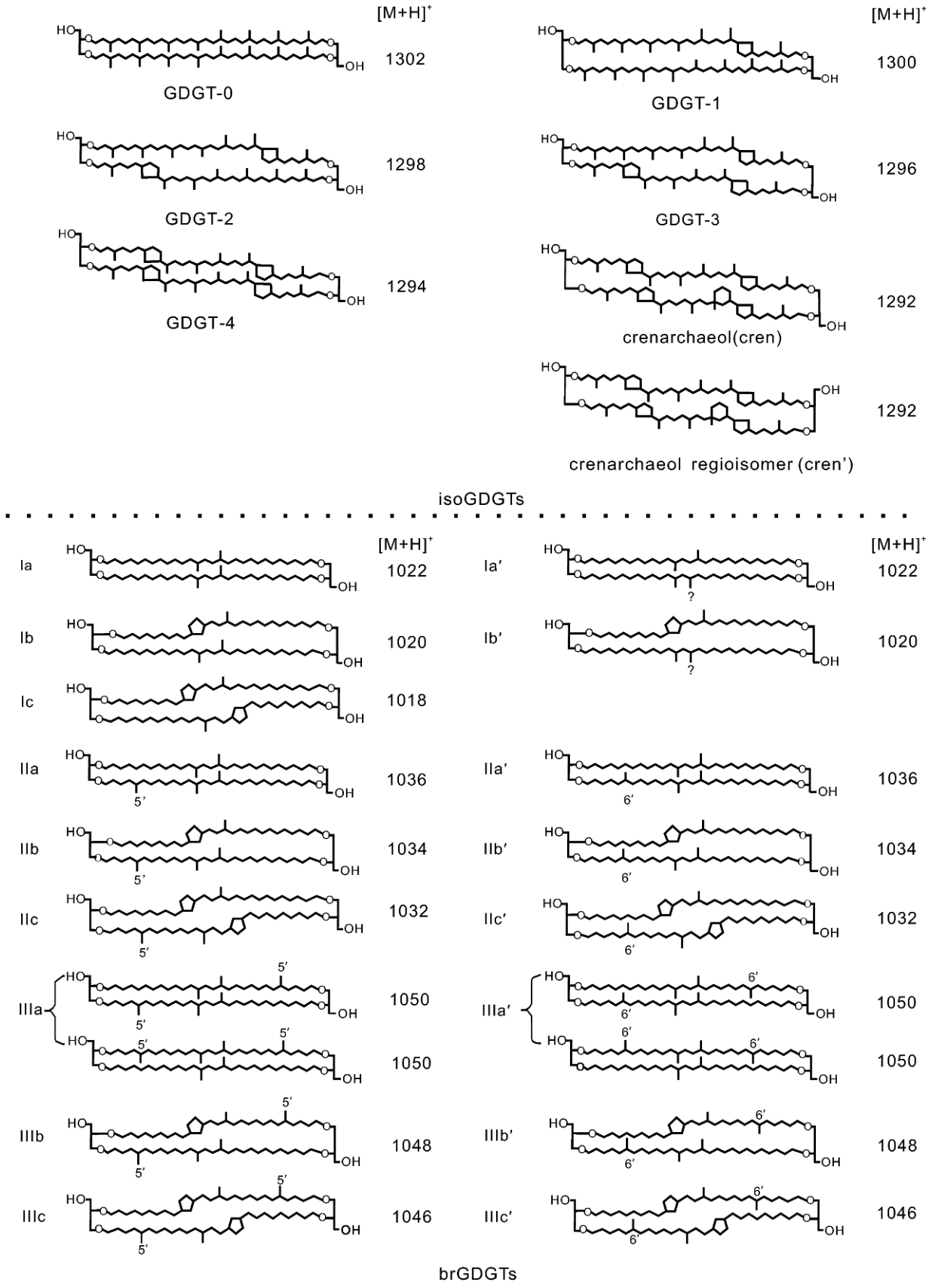

Figure 1 The structures of GDGTs (isoGDGTs and brGDGTs are shown above and below the dash line, respectively. Note that the glycerol arrangement in archaeal isoGDGTs is tentative).

al., 2014a; Wang H et al., 2016). By extension, MBT'_{5me} was also suggested to be a proxy for the reconstruction of paleoaltimetry (Yang et al., 2015). In some specific regions, e.g. the Qinghai-Tibetan Plateau (QTP), $MBT_{5/6}$, appeared to be more accurate in inferring the MAT than MBT'_{5me} (Ding et al., 2015).

Although the application of soil GDGTs to the reconstruction of paleoaltimetry has been proposed, this remains to be tested in more altitudinal transects. Due to a large spatial heterogeneity in the terrestrial environments, the same GDGT-based proxies may show distinct response to environmental variables in different regions (Zheng et al., 2016). Many previous studies showed the complexity in the use of GDGT proxies in soils (e.g. Liu et al., 2013; Yang et al., 2014b, 2016) and lakes (e.g. Dang et al., 2016a; Wang M D et al., 2016). The altitudinal transects of mountains from different climatic zones can provide unique opportunities for studying the response of GDGTs to multiple environmental variables. To date, the GDGT proxies have been tested in altitudinal transects with warm-humid and cold-dry climate, including Mt. Shennongjia (Yang et al., 2016) and Mt. Jianfengling (Yang et al., 2010), Mt. Xiangpi (Liu et al., 2013) and QTP (Ding et al., 2015). However, it is still unclear how the GDGT-based proxies respond to the environmental gradients under cold-humid climate. Here, we collected soils from Mt. Changbai, which has a typical cold-humid climate, to investigate the response of GDGTs in surface soils to environmental factors along an altitudinal transect.

2 Materials and methods

2.1 Study site

Mt. Changbai is a dormant volcano located in the southeast of Jilin Province (Figure 2a). It is the border between China and the democratic people's republic of Korea (North Korea). Mt. Changbai has a typical cold-humid climate (Table 1). Moss and lichen can be found in the forest. As the highest mountain of the eastern Eurasia continent, Mt. Changbai has a typical vertical zonation of plants: broadleaf-conifer mixed forest in the piedmont, the dark coniferous forests and *betula ermaniis* forest at relatively higher altitudes, and tundra on the top of the mountain. Dark brown soils in the Mt. Changbai are rich in organic matter with relatively high soil water content (SWC) and relatively low soil pH (Table 2). Soils are developed on the basalt erupting from the volcano hundreds of years ago. On the top of the mountain, soils are only sporadically distributed due to a poor weathering of basalt in the freezing environment.

2.2 Sample preparation

Surface soil samples were collected along an altitudinal transect of Mt. Changbai at an altitude interval of about 100 m (Figure 2b). Five subsamples were collected after the removal of the litter layer and were combined to form a composite sample. The *in situ* air and soil temperatures at each site were measured using a digital thermometer (±0.5° C). Altitude was obtained from a portable GPS (Garmin) with a precision of ±3 m. The MAT and mean annual precipitation (MAP) for each sampling site can be estimated according to the linear relationship of MAT and MAP with altitude for 6 meteorological stations nearby: Panshi (42°58′ N, 126°03′E), Huandian (42°57′N, 126°42′E), Jingyu (42° 21′N, 126°49′E), Donggang (42°06′N, 127°34′E), Tianchi (42°01′N, 128°05′E), Yanji (42°53′N, 129°28′E) (1970–2000):

$$\mathrm{MAT}(^{\circ}\mathrm{C}) = -0.005 \times \mathrm{Altitude} + 6.587 \quad (R^2 = 0.98,\ p < 0.001), \tag{1}$$

$$\mathrm{MAP}(\mathrm{mm}) = 0.067 \times \mathrm{Altitude} + 549.3 \quad (R^2 = 0.80,\ p < 0.001). \tag{2}$$

Note that the eq. (2) didn't include the meteorological data from Panshi station.

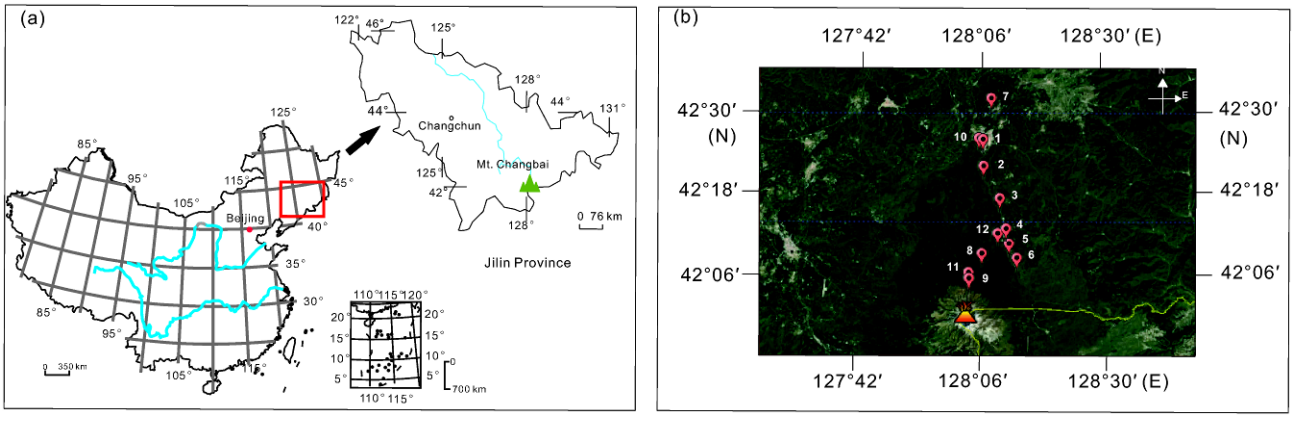

Figure 2 The location of sampling. (a) The location of Mt. Changbai [the map of China [GS (2006) 2125] is used]; (b) the location of sampling sites.

Samples were transported to the laboratory and stored at −20°C immediately after being weighed (W_o). Samples were then freeze dried and weighted again to obtain the dry weight (W_d). Soil water content (SWC) can be calculated from the eq. (3):

$$\mathrm{SWC}= (W_o - W_d) / W_o. \quad (3)$$

The dried samples were ground into powder. Five grams of each sample was mixed with 12.5 mL water and centrifuged to allow for the phase separation. The pH of supernatant was measured using a pH meter (×3) and the average value for the three measurements was used as the final pH of the soils (Table 2).

An aliquot of each sample was extracted with a mixture of dichloromethane (DCM) and methanol (MeOH) (9:1, *v*/*v*) in a ultrasonic water bath (×5) to obtain the total lipid extract (TLE). The TLE was condensed by a rotary evaporator to a volume of 3−4 mL and dried under a gentle stream of nitrogen gas. The TLE was separated into apolar and polar lipids on a column filled with activated silica with *n*-hexane and DCM:MeOH=1:1 (*v*/*v*) as the eluents, respectively. The polar lipid was base hydrolyzed for 2 h at 80°C, and the neutral fraction was obtained by extracting the solutions with *n*-hexane for 5 times. The neutral fraction, containing GDGTs, was filtered with 0.45 μm PTFE syringe filter to remove the particles and then dried under the nitrogen gas.

GDGTs were analyzed using an Agilent 1200 high performance liquid chromatogram and triple quadruple mass spectrometer (HPLC-MS/MS) equipped with an autosampler and a Masshunter workstation. Samples were spiked with a known amount of internal standard, C_{46} GTGT prior to injection (Huguet et al., 2006). Sample was re-dissolved in 300 μl of *n*-hexane: ethyl acetate (EtOA) (84:16; *v*/*v*), and the injection volume was 10 μL. The liquid chromatography method followed Yang et al. (2015). The isomers of brGDGTs were separated using two silica columns (150 mm ×2.1 mm, 1.9 μm, Thermo Finnigan; USA) in tandem fixed at 40°C. A constant flow rate of 0.2 mL min^{-1} was used. Samples were eluted with *n*-hexane (A) and EtOA (B) (84:16; *v*/*v*) isocratically for the first 5 min. Then the following elution gradient was used: 82% A and 18% B for 60 min, %B increased to 100% for the next 21 min and maintained for 4 min. 84 %A and 16% B was used to wash the column for 30 min. GDGTs were detected using the single ion monitoring (SIM), targeting *m/z* 1302, 1300, 1298, 1296, 1292, 1050, 1048, 1046, 1036, 1034, 1032, 1022, 1020, 1018 and 744. The nebulizer pressure and temperature were 60 psi and 400°C, respectively. The flow rate of the drying gas (N_2) was 6 L min^{-1} at 200°C. The capillary voltage was 3500 V, and the corona current was 5 μA (~3200 V). We assumed a same response factor between GDGTs and C_{46} GTGT in the mass spectrometer. The abundance of each GDGT compound was determined by the comparison of peak areas of GDGTs to that of C_{46} GTGT in the extracted ion chromatography.

2.3 Calculation of GDGT-based proxies

TEX_{86} was calculated according to Schouten et al. (2002):

$$\mathrm{TEX}_{86} = (\mathrm{GDGT{-}2} + \mathrm{GDGT{-}3} + \mathrm{cren}') / (\mathrm{GDGT{-}1} + \mathrm{GDGT{-}2} + \mathrm{GDGT{-}3} + \mathrm{cren}'), \quad (4)$$

where cren′ represents crenarchaeol regioisomer.

The calculation of MBT, MBT′ and CBT followed Weijers et al. (2007) and Peterse et al. (2012):

$$\mathrm{MBT}= (\mathrm{Ia}+\mathrm{Ia}'+\mathrm{Ib}+\mathrm{Ib}'+\mathrm{Ic}) / (\mathrm{Ia}+\mathrm{Ia}'+\mathrm{b}+\mathrm{Ib}'+\mathrm{c}+\mathrm{IIa}+\mathrm{IIa}'+\mathrm{Ib}+\mathrm{IIb}'+\mathrm{Ic} +\mathrm{IIc}'+\mathrm{IIa}+\mathrm{IIIa}'+\mathrm{IIb}+\mathrm{IIIb}'+\mathrm{IIc}+\mathrm{IIc}'), \quad (5)$$

$$\mathrm{CBT}= -\log[(\mathrm{Ib}+\mathrm{Ib}'+\mathrm{IIb}+\mathrm{IIb}') / (\mathrm{Ia}+\mathrm{Ia}'+\mathrm{IIa}+\mathrm{IIa}')]. \quad (6)$$

$$\mathrm{MBT}' = (\mathrm{Ia}+\mathrm{Ia}'+\mathrm{b}+\mathrm{Ib}'+\mathrm{c}) / (\mathrm{Ia}+\mathrm{Ia}'+\mathrm{Ib}+\mathrm{Ib}'+\mathrm{c}+\mathrm{IIa}+\mathrm{IIa}'+\mathrm{Ib} +\mathrm{IIb}'+\mathrm{Ic}+\mathrm{Ic}'+\mathrm{IIa}+\mathrm{IIIa}'). \quad (7)$$

MBT'_{5me}, MBT'_{6me}, CBT_{5me}, and CBT_{6me} were calculated according to De Jonge et al. (2014a). $\mathrm{IR}_{x'}$ was calculated according to De Jonge et al. (2014b).

$$\mathrm{MBT}'_{5me} = (\mathrm{Ia}+\mathrm{Ia}'+\mathrm{Ib}+\mathrm{Ib}'+\mathrm{Ic}) / (\mathrm{Ia}+\mathrm{Ia}'+\mathrm{Ib}+\mathrm{Ib}'+\mathrm{Ic}+\mathrm{IIa}+\mathrm{IIb}+\mathrm{IIc}+\mathrm{IIIa}). \quad (8)$$

$$\mathrm{MBT}'_{6me} = (\mathrm{Ia}+\mathrm{Ia}'+\mathrm{Ib}+\mathrm{Ib}'+\mathrm{Ic}) / (\mathrm{Ia}+\mathrm{Ia}'+\mathrm{Ib}+\mathrm{Ib}'+\mathrm{Ic}+\mathrm{IIa}'+\mathrm{IIb}'+\mathrm{IIc}'+\mathrm{IIIa}'). \quad (9)$$

$$\mathrm{CBT}_{5me} = -\log[(\mathrm{Ib}+\mathrm{Ib}'+\mathrm{IIb}) / (\mathrm{Ia}+\mathrm{Ia}'+\mathrm{IIa})]. \quad (10)$$

Table 1 Different climate types in the previous studies[a)]

Site	Altitude (m)	MAT (°C)	Soil pH	SWC	Climate type	Reference
Mt. Jianfengling	86–1405	16–24	4.03−6.20	–	Warm-humid	Yang et al., 2010
Mt. Shennongjia	316–2907	1–16.7	5.03−8.01	7.8–45%	Warm-humid to cold-humid	Yang et al., 2016
QTP	3066–5418	−5.5–7.6	6.22−8.37	–	Cold-dry	Ding et al., 2015
Mt. Xiangpi	3250–4104	−8.2–0.4	7.3−8.1	–	Cold-dry	Liu et al., 2013
Mt. Gongga	1180–3819	−1.5–14.3	4.4−7.9	–	Cold-humid	Peterse et al., 2009
Mt. Changbai	643–1910	−5–3	4.52−6.43	30.4−78.3%	Cold-humid	This study

a) MAT, mean annual temperature; SWC, soil water content; '–' represents data unavailable; QTP, Qinghai-Tibetan Plateau

Table 2 Sample information for the soils collected from Mt. Changbai[a)]

Sample No.	Sampling T (°C)	Sampling air T (°C)	Alt (m)	GPS	GPS	MAT_e (°C)	MAP_e (mm)	SWC	Soil pH
CB 1-1	8.2	14.8	742	42°23′55″N	128°05′29E	2.9	599	70.5%	5.54
CB 1-2	8.9	14.2	742	42°23′55″N	128°06′28″E	2.9	599	63.0%	5.15
CB 1-3	8.5	15.1	748	42°23′55″N	128°06′28″E	2.9	599	42.7%	5.49
CB 2-1	7.5	14.5	859	42°19′52″N	128°06′36″E	2.3	607	71.0%	5.30
CB 2-2	7.7	13.1	859	42°19′53″N	128°06′34″E	2.3	607	78.3%	5.25
CB 2-3	7.3	13.7	860	42°19′52″N	128°06′33″E	2.3	607	51.2%	4.61
CB 3-1	6.7	14.0	1008	42°15′10″N	128°09′48″E	1.6	617	51.7%	5.09
CB 3-2	6.9	14.6	1004	42°15′09″N	128°09′47″E	1.6	617	55.1%	6.05
CB 3-3	7.2	13.7	1005	42°15′09″N	128°09′48″E	1.6	617	56.2%	5.68
CB 4-1	5.8	14.1	1130	42°10′48″N	128°11′01″E	0.9	625	61.8%	5.96
CB 4-2	5.7	13.0	1134	42°10′48″N	128°11′02″E	0.9	625	46.6%	5.47
CB 4-3	5.9	13.9	1139	42°10′48″N	128°11′03″E	0.9	626	54.4%	5.70
CB 5-1	7.3	10.8	1248	42°08′35″N	128°11′34″E	0.4	633	50.5%	4.96
CB 5-2	6.9	12.0	1248	42°08′34″N	128°11′34″E	0.4	633	49.5%	5.46
CB 5-3	8.6	12.0	1249	42°08′35″N	128°11′34″E	0.3	633	41.0%	4.55
CB 6-1	5.6	7.9	1349	42°06′32″N	128°13′04″E	−0.2	640	59.7%	4.67
CB 6-2	6.6	7.9	1349	42°06′31″N	128°13′04″E	−0.2	640	63.7%	4.87
CB 6-3	7.5	7.9	1350	42°06′31″N	128°13′03″E	−0.2	640	73.5%	4.52
CB 7-1	9.3	14.9	643	42°30′03″N	128°08′02″E	3.4	592	47.8%	5.87
CB 7-2	11.9	14.9	646	42°30′05″N	128°08′02″E	3.4	593	30.4%	6.13
CB 7-3	11.9	14.0	646	42°30′05″N	128°08′02″E	3.4	593	45.1%	6.43
CB 8-1	–	–	1350	42°07′09″N	128°06′23″E	−0.2	640	–	4.40
CB 9-1	–	–	1910	42°03′40″N	128°04′01″E	−3.0	677	–	4.68
CB 9-2	–	–	1910	42°03′40″N	128°04′01″E	−3.0	677	–	4.71
CB 10-1	–	–	790	42°24′06″N	128°05′39″E	2.6	602	–	4.99
CB 10-2	–	–	790	42°24′06″N	128°05′39″E	2.6	602	–	5.03
CB 11-1	–	–	1700	42°04′29″N	128°03′54″E	−1.9	663	–	4.75
CB 11-2	–	–	1700	42°04′29″N	128°03′54″E	−1.9	663	–	4.73
CB 12-1	–	–	1200	42°10′07″N	128°09′25″E	0.6	630	–	4.71

a) T, temperature; Alt, altitude; MAT_e, estimated mean annual temperature; MAP_e, estimated mean annual precipitation; '–' represents data unavailable.

$$CBT_{6me} = -\log[(Ib+Ib'+IIb')/(Ia+Ia'+IIa')]. \quad (11)$$

$$IR_{x'} = x'/(x+x'), \quad (12)$$

where, x represents 5-methyl brGDGTs, x' represents 6-methyl brGDGTs.

$MBT_{5/6}$, previously defined by Ding et al. (2015), was calculated according to the equation:

$$MBT_{5/6} = (Ia+Ia'+Ib+Ib'+Ic+IIa')/(Ia+Ia'+Ib+Ib'+Ic+IIa+IIa'+IIb+IIc+IIIa+IIIa'). \quad (13)$$

3. Results and discussion

3.1 The distribution of GDGTs and GDGT-based proxies

The relative abundances of brGDGTs for the soils from Mt. Changbai were much higher than those of isoGDGTs (Figure 3). GDGT-0 and crenarchaeol were generally the major isoGDGT components, with an average abundance of 54.2% and 24.9%, respectively (Figure 4a). GDGT-Ia, IIa and IIa′ accounted for the major proportions of brGDGTs, with an average abundance of 39.7%, 32.3% and 10.3%, respectively (Figure 4b) (The relative abundance of isoGDGTs and brGDGTs are shown in Appendix (Tables S1 and S2, http://link.springer.com), respectively; the GDGT proxies are shown in Table 3).

TEX_{86} for these samples varied from 0.43 to 0.75. No clear relationship between TEX_{86} and MAT can be found. MBT'_{5me}, MBT'_{6me}, and $MBT_{5/6}$ were in the range of 0.38–0.65, 0.39–0.97 and 0.40–0.66, respectively (Table 3). We cannot find a clear relationship between MBT'_{5me} and MAT or soil pH (Figure 5). Likewise, the relationship between $MBT_{5/6}$ and

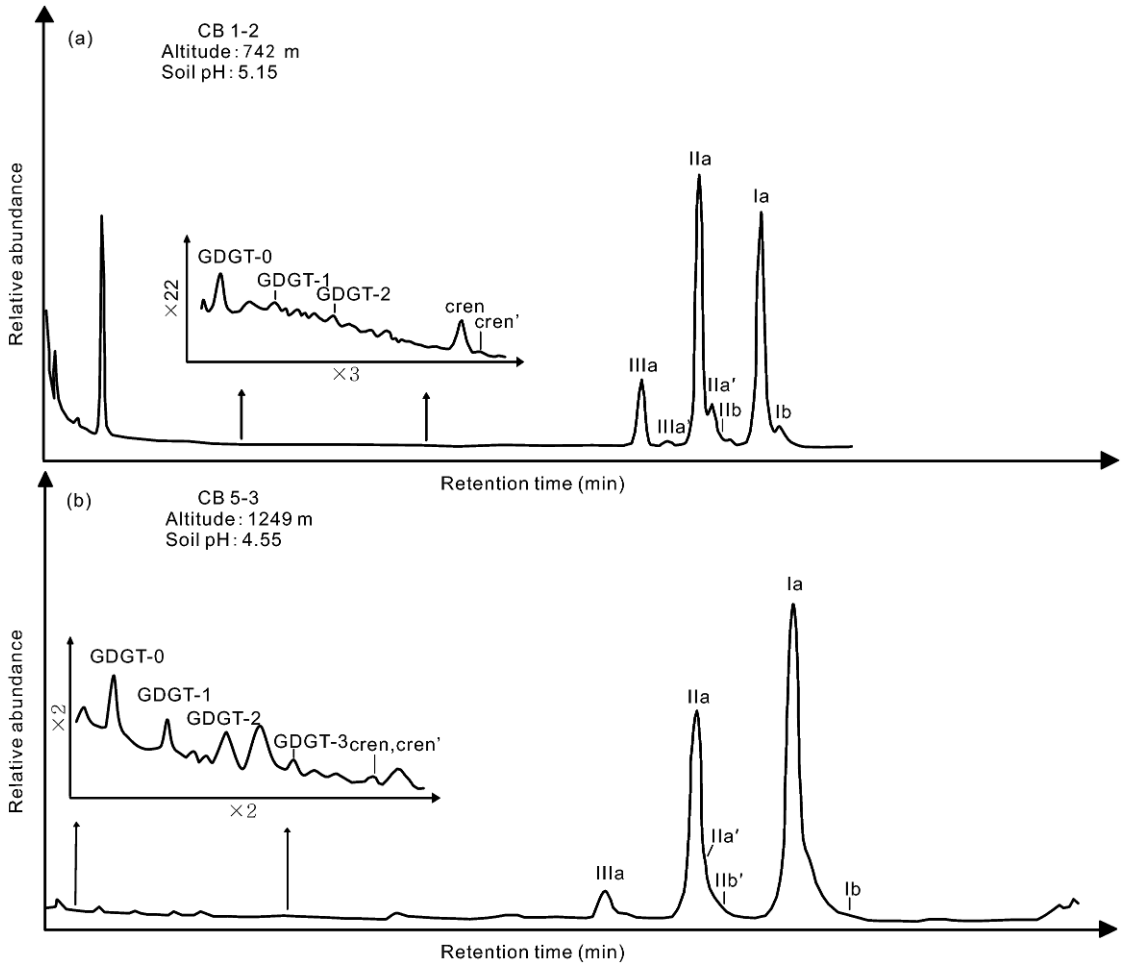

Figure 3 The total ion chromatography of GDGTs for selected samples (CB 1-2 and CB 5-3) from Mt. Changbai.

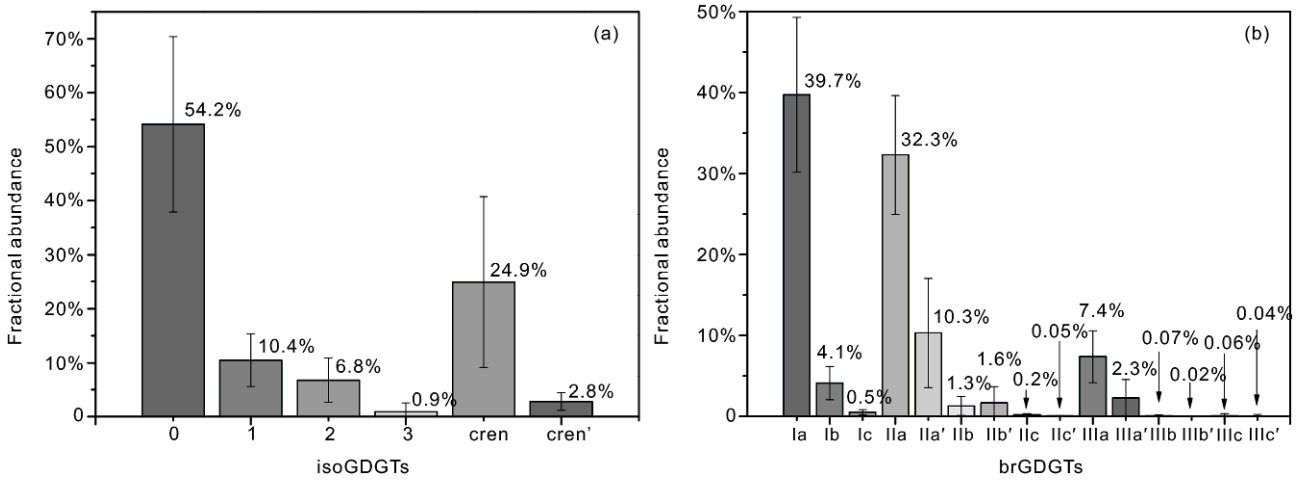

Figure 4 The average abundance of (a) isoGDGTs and (b) brGDGTs for all the soils collected from Mt. Changbai.

MAT was poor. In contrast, MBT'_{5me} exhibited a significant negative correlation with SWC (R^2=0.54, p<0.001, an outlier was excluded). MBT'_{6me} showed a negative correlation with soil pH (R^2=0.88, p<0.001).

CBT, CBT_{5me} and CBT_{6me} ranged from 0.43–1.64, 0.40–1.70, and 0.4–1.51, respectively (Table 3). All of them showed a close relationship with soil pH (Figure 5) with similar regression lines (Figure 6a). $IR_{IIa'}$ and $IR_{IIIa'}$ varied from 0.01–0.64 and 0.02–0.66, respectively. They were shown to be significantly dependent on soil pH (Figures 5

Table 3 GDGT-based proxies for soils along an altitudinal transect of Mt. Changbai[a)]

No.	Sample No.	TEX_{86}	MBT′	MBT'_{5me}	MBT'_{6me}	$MBT_{5/6}$	CBT	CBT_{5me}	CBT_{6me}	$IR_{IIa'}$	$IR_{IIIa'}$
1	CB 1-1	–	0.38	0.48	0.64	0.54	0.93	0.94	0.82	0.33	0.30
2	CB 1-2	0.53	0.42	0.46	0.82	0.50	1.32	1.33	1.16	0.16	0.10
3	CB 1-3	0.43	0.41	0.52	0.65	0.58	0.82	0.85	0.72	0.35	0.38
4	CB 2-1	0.56	0.37	0.41	0.78	0.45	1.12	1.14	0.93	0.17	0.13
5	CB 2-2	–	0.34	0.38	0.80	0.41	1.29	1.31	1.07	0.13	0.09
6	CB 2-3	–	0.58	0.61	0.92	0.62	1.39	1.42	1.26	0.11	0.11
7	CB 3-1	–	0.50	0.61	0.75	0.64	0.99	1.03	0.89	0.32	0.36
8	CB 3-2	–	0.40	0.53	0.62	0.58	0.76	0.81	0.67	0.37	0.44
9	CB 3-3	–	0.47	0.57	0.73	0.61	1.06	1.09	0.96	0.31	0.33
10	CB 4-1	0.73	0.38	0.51	0.59	0.58	0.90	0.93	0.79	0.41	0.39
11	CB 4-2	0.75	0.42	0.50	0.72	0.56	1.04	1.08	0.92	0.28	0.25
12	CB 4-3	–	0.39	0.49	0.65	0.55	0.90	0.93	0.79	0.33	0.28
13	CB 5-1	–	0.55	0.58	0.93	0.59	1.33	1.35	1.16	0.08	0.07
14	CB 5-2	–	0.47	0.54	0.77	0.58	1.21	1.23	1.11	0.26	0.19
15	CB 5-3	–	0.61	0.65	0.91	0.66	1.45	1.49	1.32	0.15	0.04
16	CB 6-1	0.75	0.52	0.55	0.91	0.56	1.61	1.70	1.45	0.10	0.13
17	CB 6-2	0.61	0.47	0.53	0.82	0.56	1.36	1.41	1.16	0.18	0.18
18	CB 6-3	–	0.58	0.61	0.94	0.62	1.64	1.69	1.51	0.10	0.06
19	CB 7-1	0.63	0.34	0.53	0.50	0.60	0.56	0.55	0.51	0.52	0.56
20	CB 7-2	0.68	0.38	0.59	0.52	0.66	0.72	0.71	0.68	0.56	0.57
21	CB 7-3	0.68	0.29	0.54	0.39	0.61	0.43	0.40	0.41	0.64	0.66
22	CB 8-1	–	0.55	0.58	0.91	0.60	1.52	1.60	1.36	0.12	0.04
23	CB 9-1	–	0.39	0.40	0.97	0.40	1.48	1.52	1.23	0.01	0.02
24	CB 9-2	–	0.40	0.43	0.86	0.44	1.62	1.59	1.33	0.10	0.13
25	CB 10-1	0.52	0.48	0.55	0.79	0.59	1.01	1.02	0.90	0.25	0.19
26	CB 10-2	0.55	0.48	0.55	0.78	0.59	1.02	1.02	0.90	0.26	0.18
27	CB 11-1	–	0.36	0.38	0.86	0.41	1.54	1.55	1.25	0.09	0.05
28	CB 11-2	–	0.43	0.46	0.87	0.48	1.37	1.46	1.14	0.11	0.06
29	CB 12-1	–	0.54	0.57	0.89	0.60	1.37	1.36	1.22	0.16	0.05

a) '–': GDGT-0/cren>2

and 6b; Table 3).

To further assess the applicability of $IR_{IIa'}$ and $IR_{IIIa'}$ as pH proxies in more diverse environments, the published data for Mt. Shennongjia (Yang et al., 2016), QTP (Ding et al., 2015) and the global soils (De Jonge et al., 2014a) were combined with data in this study. These two indices still exhibited significant correlations with soil pH in global soils from a variety of environments (Figure 6c and 6d), indicating that $IR_{IIa'}$ and $IR_{IIIa'}$ can be applied to different types of soils globally and are more reliable than CBT.

3.2 Influence of archaeal community and seasonality on TEX_{86}

TEX_{86} for Mt. Xiangpi (Liu et al., 2013), Mt. Shennongjia (Yang et al., 2016), Mt. Jianfengling (Yang et al., 2010) all showed significant correlations with altitude or MAT, although these three mountains have distinct climates. The regression lines for them are different, indicating that some other factors may also have an influence on the relationship between TEX_{86} and MAT.

Unlike above three mountains, TEX_{86} for soils from Mt. Changbai were scattered and showed no correlation with MAT (Figure 7a). Blaga et al. (2008) proposed the ratio of GDGT-0/cren as a proxy for the contribution of methanogens in the archaeal community. The ratio>2 means methanogens and Bathyarchaeota contribute a significant amount of isoGDGTs, and vice versa (Besseling et al., 2017). Approximately 59% of samples for Mt. Changbai showed a GDGT-0/cren ratio>2. Likewise, the majority of the samples from Mt. Jianfengling also showed a GDGT-0/cren ratio>2. This is likely because Mt. Jianfengling and Changbai both have very humid climate and soils (Yang et al., 2010). In contrast, only 4% of the samples showed GDGT-0/cren>2 at

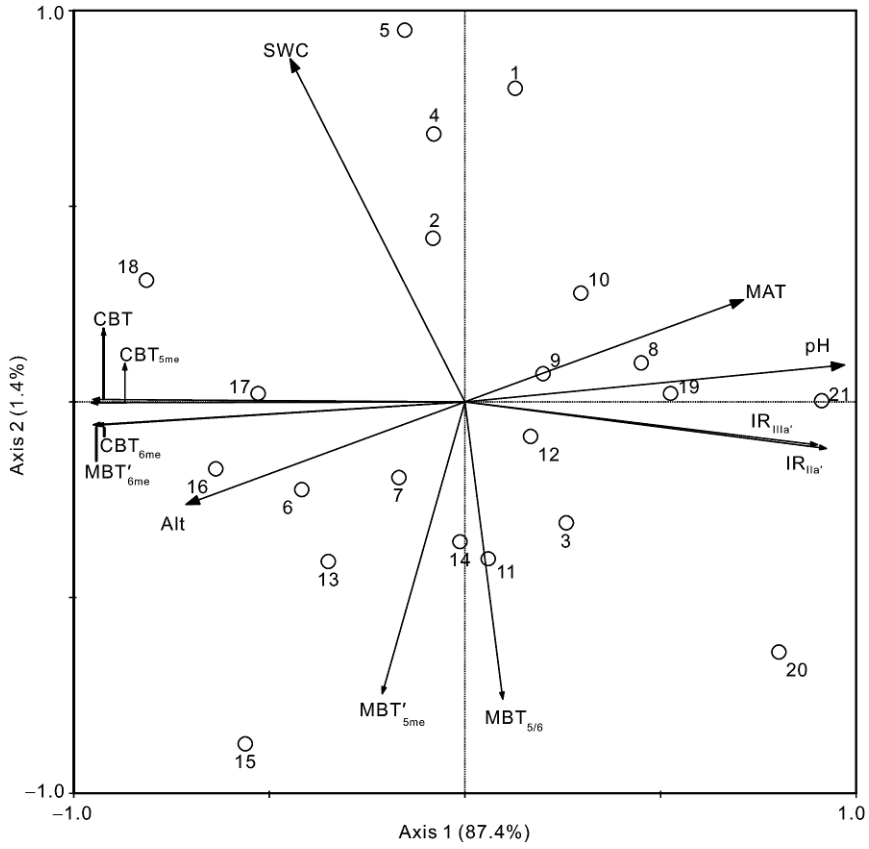

Figure 5 Redundancy analysis (RDA) showing the relationship between environmental factors and the brGDGT-based proxies for soils from Mt. Changbai. MAT, mean annual temperature; SWC, soil water content; Alt, altitude. The numbers denote the corresponding samples in Table 3.

Mt. Shennongjia, where the climate is less humid than both Mt. Changbai and Jianfengling (Yang et al., 2016).

The distribution of archaeal isoGDGTs and bacterial brGDGTs changed with soil pH (Figure 3). The relative abundance of GDGT-0 was higher in the soils with lower soil pH whereas the relative abundance of crenarchaeol was higher in the circumneutral environments. The humic substance accumulates in the cold and humid forest at Mt. Changbai due to a relatively low microbial activity, leading to a high soil organic carbon content and relatively low soil pH. Soils at Mt. Changbai are thus favorable to the growth of methanogens and Bathyarchaeota that can produce more GDGT-0. In addition, acidic Thaumarchaeota and Thaumarchaeota Group I.1c and Group I.3 occur in a high abundance in the acidic forest soils (Lehtovirta et al., 2009, 2016; Cao et al., 2012). These archaea, e.g. *Nitrosotalea devanaterra*, an acidophilic Thaumarchaeotal isolate, can produce more abundant GDGT-4 than crenarchaeol, which is different from other archaea falling into Thaumarchaeota Group I.1a and Group I.1b (Lehtovirta et al., 2016). Besides, some other studies showed that Thermoplasma and methanogens might also biosynthesize crenarchaeol (Li et al., 2017). Therefore, it is likely that soil pH-induced changes in the archaeal community may affect the composition of isoGDGTs and in turn have an influence on the TEX_{86} value. The complex archaeal communities at soils of Mt. Changbai may be one of the causes of the weak correlation between TEX_{86} and MAT for the cold and humid climate.

The average TEX_{86} value at lower altitudes (MAT>2°C) was larger than that at higher altitudes (MAT<2°C) (Figure 7b). This can be explained by an increased seasonal production of archaea in the colder soils. Most microbes prefer to inhabit temperate environments, and their growth may be significantly suppressed in the frozen soils. The MAT is very low and the SWC is relatively high at the peak of Mt. Changbai, where the soils keep frozen during most seasons of a year. Only the temperature signal when the soils are not frozen and archaea are actively growing can be recorded by TEX_{86}. In contrast, soil will not be frozen at lower altitudes and the TEX_{86} can record the temperature signal throughout a year. This may lead to systematically higher TEX_{86} values at higher than low altitudes. We complied the published TEX_{86} values for soils (Yang et al., 2010; Liu et al., 2013; Blyth et al., 2014; Yang et al., 2016) and the pure cultures of Group I.1b Thaumarchaeota (Pitcher et al., 2010; Sinninghe Damsté et al., 2012; Elling et al., 2017) and plotted them against MAT or growing temperatures. TEX_{86} for data points with MAT<2°C were higher than those with MAT>2°C (Figure 7c). For those data points with MAT<2°C, the months from April to October, when the mean temperature of each month

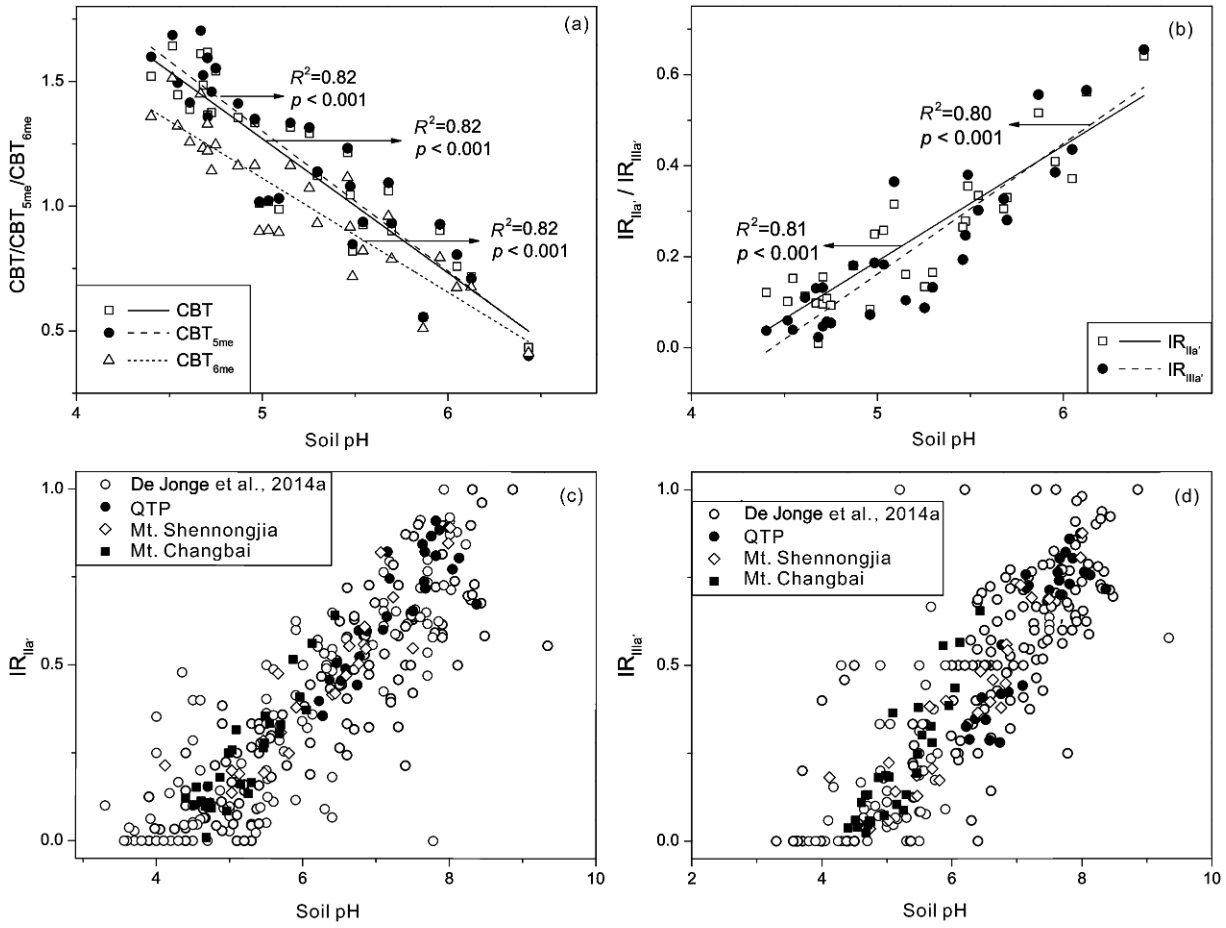

Figure 6 (a) Linear correlations between CBT, CBT$_{5me}$, and CBT$_{6me}$ for soils from Mt. Changbai and soil pH; (b) Liner correlations between IR$_{IIa'}$, IR$_{IIIa'}$ for soils from Mt. Changbai and soil pH; the linear relationship of soil pH with (c) IR$_{IIa'}$ and (d) IR$_{IIIa'}$ for the complied dataset including data from this study, the QTP (Ding et al., 2015), Mt. Shennongjia (Yang et al., 2016) and the global soils (De Jonge et al., 2014a).

is larger than 0°C, was favorable to the growth of archaea. If the MAT for Mt. Xiangpi and higher altitudes of Mt. Changbai (MAT<2°C) was substituted with the mean temperature for these months, i.e., the growing season temperature, TEX$_{86}$ showed a significant correlation with the mean growing season temperatures (Figure 7d). As archaea producing isoGDGTs in these soils mainly belong to Group I.1b Thaumarchaeota, it is reasonable to observe that data points for the pure cultures of Thaumarchaeota Group I.1b at different temperatures were plotted near the regression line. We can therefore obtain a global calibration of TEX$_{86}$ for the growing season temperature reconstruction in soil environments:

$$T = 85.19 \times \mathrm{TEX}_{86} - 46.30 \,(R^2 = 0.84,\ p < 0.001). \quad (14)$$

Compared with the global calibration of TEX$_{86}$ for marine and lake environments (Table 4), the slope of eq. (14) is higher and the intercept is lower, indicating a distinct response of archaeal membrane lipids to temperature between the aquatic and soil environments. This is likely because the major isoGDGT-producing archaea in soils belong to Group I.1b Thaumarchaeota but the dominant archaea in marine and deep lake environments fall into Thaumarchaeota Group I.1a (Schouten et al., 2013). This global calibration (eq. (14)) may be potentially useful in the quantitative reconstruction of paleotemperature in the loess-paleosol.

3.3 Impact of SWC on the methylation index of brGDGTs

A number of previous studies suggested that MBT′$_{5me}$ and MBT$_{5/6}$ correlated with MAT (De Jonge et al., 2014a; Yang et al., 2015; Ding et al., 2015). However, MBT′$_{5me}$ and MBT$_{5/6}$ for Mt. Changbai exhibited no correlation with MAT (Figure 5) and were more variable than data for QTP (cold-dry climate), Mt. Gongga (cold-humid) and Mt. Shennongjia (warm-humid) (Figure 8a and 8b). This is largely because Mt. Changbai have low MAT and humid climate. In fact, data for Mt. Gongga, which also has a cold and humid climate, showed a large scatter when MAT is <5°C.

After removal of an outlier from the data set for Mt. Changbai (CB 6-3), MBT′$_{5me}$ and MBT$_{5/6}$ showed significant

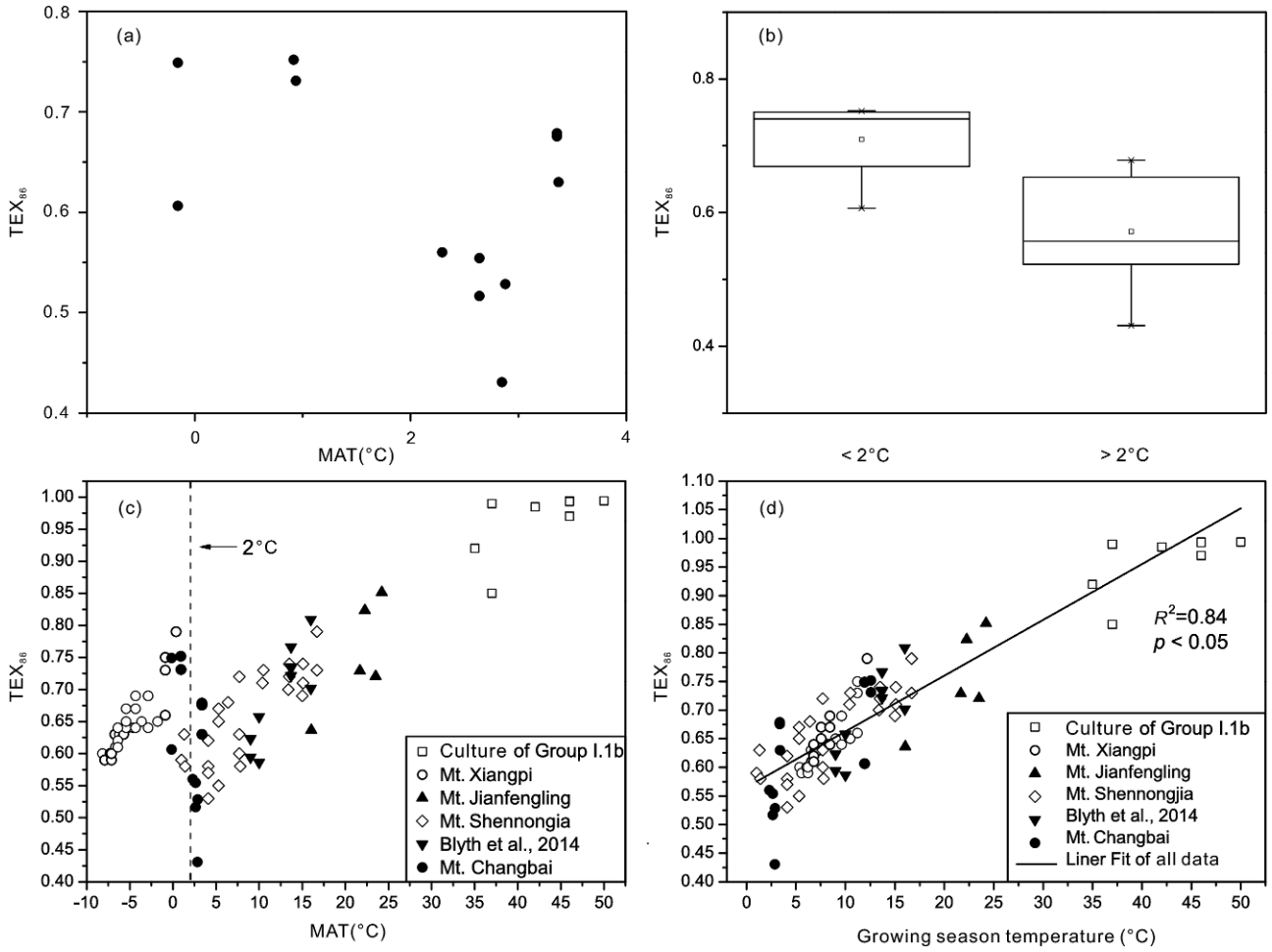

Figure 7 (a) Correlation between TEX_{86} (data with GDGT-0/cren<2) for Mt. Changbai and MAT (mean annual temperature); (b) comparison of TEX_{86} between data points with MAT<2°C and >2°C in the box plot; (c) correlation between MAT and TEX_{86} from the compiled data for soils from Mt. Xiangpi (Liu et al., 2013), Mt. Jianfengling (Yang et al., 2010), Mt. Shennongjia (Yang et al., 2016), and soils recovered from caves in the UK and Australia (Blyth et al., 2014) and for the pure cultures of Group I.1b Thaumarchaeota (Pitcher et al., 2010; Sinninghe Damsté et al., 2012; Elling et al., 2017); (d) a global calibration of TEX_{86} and growing season temperature based on data from Mt. Xiangpi (Liu et al., 2013), Mt. Jianfengling (Yang et al., 2010), Mt.Shennongjia (Yang et al., 2016) and soils recovered from caves in the UK and Australia (Blyth et al., 2014) and for the pure cultures of Group I.1b Thaumarchaeota (Pitcher et al., 2010; Sinninghe Damsté et al., 2012; Elling et al., 2017). Note that the growing seasons include May to September at Mt. Xiangpi, and April to October at an altitude from 1130 to 1350 m for Mt. Changbai.

Table 4 The published calibrations of TEX_{86} for temperature reconstruction[a)]

The calibration equation of TEX_{86}	Sample	Reference
$SST=56.2\times TEX_{86}-10.8$	Sea sediments	Kim et al., 2008
$SLST=50.8\times TEX_{86}-10.4$	Lake sediments	Powers et al., 2010
$WLST=57.3\times TEX_{86}-17.5$	Lake sediments	Powers et al., 2010

a) SST, sea surface temperature; SLST, lake surface temperature in summer; WLST, lake surface temperature in winter.

correlations with SWC (R^2=0.54 and 0.68, respectively, p of them both<0.001) (Figure 8c and 8d). This is also the case for Mt. Shennongjia (MBT'_{5me} and $MBT_{5/6}$ vs. SWC, R^2 0.57 and 0.49, respectively, p both<0.001) (Figure 8e and 8f). Although it appears that MBT'_{5me} and $MBT_{5/6}$ for Mt. Changbai and Mt. Gongga both exhibited correlations with SWC, SWC for Mt. Shennongjia was correlated with MAT (R^2=0.61, p<0.001) whereas SWC for Mt. Changbai had no relationship with MAT (R^2=0.01, p>0.05). Therefore, the correlation between MBT'_{5me} and SWC for Mt. Shennongjia was caused by the correlation between SWC and MAT. The relationship between MBT'_{5me} and SWC for Mt. Changbai was not impacted by MAT, indicating that SWC may affect MBT'_{5me} under cold and humid climate (MAT<5°C). In fact, temperature proxies based on microbial lipids, e.g. TEX_{86}^{L} of isoGDGTs (Kim et al., 2010), do not respond to temperature sensitively when temperature is close to 0°C. This may be due in part to the limit of the membrane lipid adjustment to the low temperature or the changes in the microbial communities when temperature decreases. SWC may cause the changes of oxygen content in soils, which also

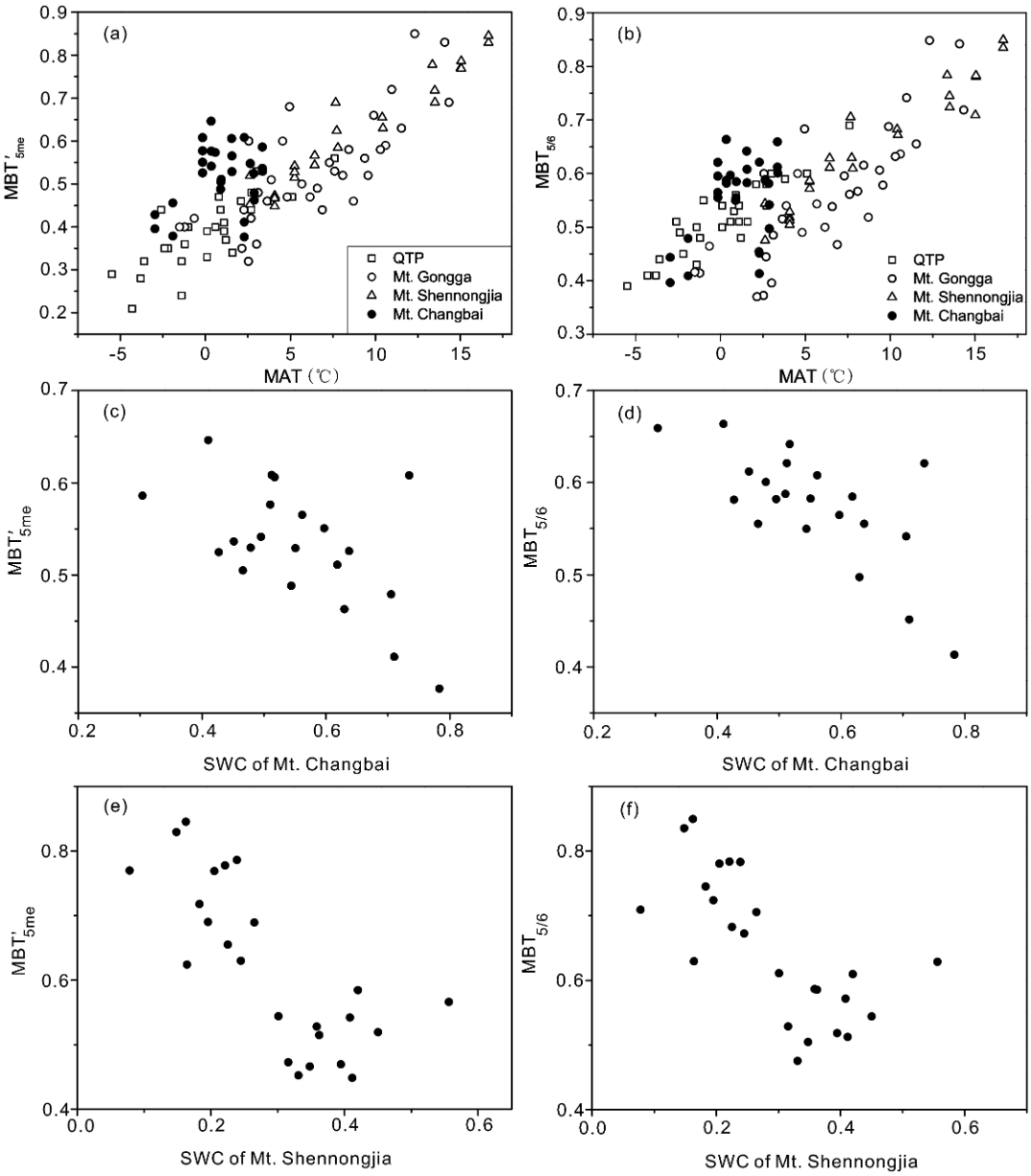

Figure 8 (a) Correlation between MBT′$_{5me}$ for QTP (Qinghai-Tibetan Plateau) (Ding et al., 2015), Mt. Gongga (De Jonge et al., 2014a), Mt. Shennongjia (Yang et al., 2015), Mt. Changbai and MAT; (b) correlation between MBT$_{5/6}$ for QTP (Qinghai-Tibetan Plateau) (Ding et al., 2015), Mt. Gongga (De Jonge et al., 2014a), Mt. Shennongjia (Yang et al., 2015), Mt. Changbai and MAT; (c) correlation between MBT′$_{5me}$ for Mt. Changbai and SWC (soil water content); (d) correlation between MBT$_{5/6}$ for Mt. Changbai and SWC (soil water content); (e) correlation between MBT′$_{5me}$ for Mt. Shennongjia and SWC (soil water content) (Yang et al., 2015); (f) correlation between MBT$_{5/6}$ for Mt. Shennongjia and SWC (soil water content) (Yang et al., 2015).

exerts a significant impact on the metabolism of bacteria in soils. As SWC is not a limiting factor for the growth of bacteria in the soils of Mt. Changbai, we speculate that SWC-induced changes in oxygen content is more likely to be the direct environmental control on MBT′$_{5me}$ and MBT$_{5/6}$.

We complied GDGT data from other three regions, i.e., QTP (Ding et al., 2015), Kunming (Lei et al., 2016), Turpan (Zang et al., 2018), which have cold-dry, warm-humid and warm-dry climate, respectively and made comparison with that for Mt. Changbai (Figure 9). Soils from the cold-dry regions showed low MBT′$_{5me}$ and MBT′$_{6me}$. In contrast, soils from the cold and humid Mt. Changbai exhibited low MBT′$_{5me}$ yet relatively higher MBT′$_{6me}$. We defined a MBT′$_{5me}$ threshold (0.65) to distinguish the warm and cold regions and a MBT′$_{6me}$ threshold (0.55) to distinguish the dry and humid regions. Figure 9 showed that MBT′$_{5me}$>0.65 and MBT′$_{6me}$ >0.55 occurred in warm-humid regions, MBT′$_{5me}$<0.65 and MBT′$_{6me}$>0.55 in cold-humid regions, MBT′$_{5me}$<0.65 and MBT′$_{6me}$<0.55 in cold-dry regions, and MBT′$_{5me}$>0.65 and MBT′$_{6me}$<0.55 in warm-dry regions. The increased dry climate can enhance the alkalinity of soils and decrease the SWC, both of which are thought to lead to a lower MBT′$_{6me}$

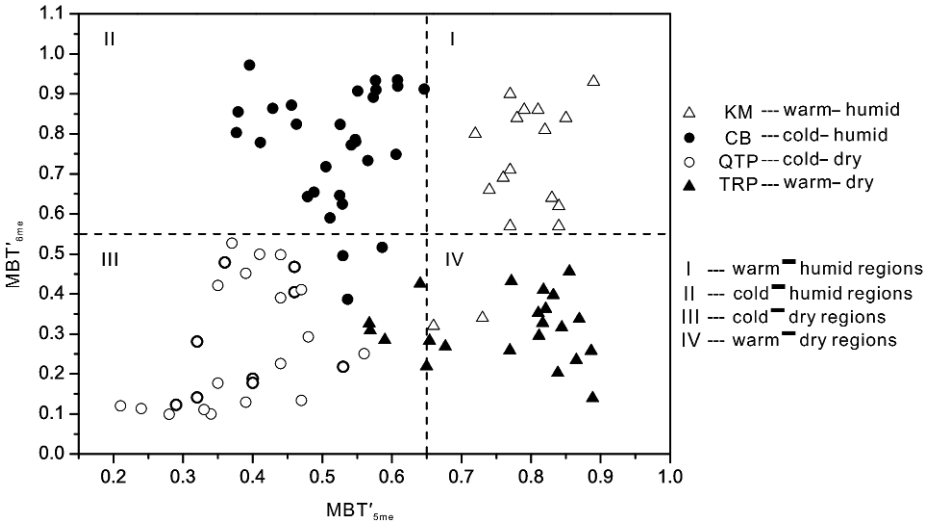

Figure 9 Cross plots of MBT'_{5me} and MBT'_{6me} , which can be used to diagnose different climate types. QTP: Qinghai-Tibetan Plateau (Ding et al., 2015), MAT −5.5–7.6°C, MAP 194–495 mm; TRP: Turpan (Zang et al., unpublished), MAT 15.1°C, MAP 1.3 mm; KM: Kunming (Lei et al., 2016), MAT 14.9°C, MAP 1012 mm; CB: Mt. Changbai (this study), MAT −3.0–3.4°C, MAP 592.4–677.5 mm, SWC 0.30–0.78.

value. Therefore, the combination of MBT'_{5me} and MBT'_{6me} can be used as a proxy to indicate different types of climates in the paleoclimate reconstruction.

3.4 The potential of MBT′/CBT in the paleoaltitude reconstruction under cold-humid climate

Although no relationship can be found between MBT'_{5me} or $MBT_{5/6}$ and MAT under cold-humid climate, the MBT′/CBT, a classic GDGT-based proxy, exhibited a significant correlation with altitude of Mt. Changbai. The calibration equation is:

$$\mathrm{Alt}(m) = 1019.85 \times \mathrm{CBT} - 1407.36 \times \mathrm{MBT}' + 552.86 \ (R^2 = 0.60, p < 0.001). \quad (15)$$

This equation is different from those for other altitudinal transects (Yang et al., 2014b), which might be caused by the differences between the lapse rates of these transects. Dang et al. (2016b) proposed the relative amount of 6-methyl brGDGTs, IR_{6me}, to distinguish the environmental control on MBT′. When IR_{6me}<0.5, MBT′ was thought to be dependent primarily on MAT. After precluding data points with IR_{6me} >0.5 (CB 7-1, CB 7-2, CB 7-3), the linear correlation between MBT′, CBT and MAT was not improved significantly:

$$\mathrm{Alt}(m) = 1014.15 \times \mathrm{CBT} - 1386.20 \times \mathrm{MBT}' + 551.98 \ (R^2 = 0.51, p < 0.001). \quad (16)$$

The premise that MBT′/CBT can be used to reconstruct altitude is that this proxy can be used to reconstruct MAT. However, the correlation between MBT′/CBT and altitude was not necessarily caused by the relationship between MBT′ and MAT for some transects. For example, MBT′ for Mt. Jianfengling and Meghalaya showed no correlation with altitude. The relationship between the MBT′/CBT and altitude was primarily dependent on the significant correlation between CBT and altitude (Yang et al., 2014b). Likewise, The reconstructed altitudes for Mt. Changbai from the eq. (15) showed a significant correlation with soil pH (R^2=0.62, p<0.001), indicating that the relationship of MBT′/CBT with altitude of Mt. Changbai was also derived from the correlation between pH and altitude. In the paleoaltimetry reconstruction, however, soil pH at different altitude may be not necessarily associated with the altitude. Therefore, in terms of paleoaltimetry reconstruction, the MBT′/CBT proxy is somewhat complex because in some cases it is CBT that causes the correlation between this proxy and altitude, rather than MBT′. The use of MBT′/CBT proxy in the paleoaltimetry reconstruction should be taken with caution.

4. Conclusions

Bacterial brGDGTs over dominated archaeal isoGDGTs in the soils from an altitudinal transect of Mt. Changbai that has a typical cold and humid climate. The ratio of GDGT-0/crenarchaeol for most soil samples were larger than 2, indicating that anaerobic methanogens or Bathyarchaeota account for a large amount of archaeal community. The seasonal production of archaea in soils from cold regions makes the response of TEX_{86} to temperature complex. MBT'_{5me} was primarily dependent on the SWC in this cold humid environment. CBT, $IR_{IIa'}$, and $IR_{IIIa'}$ all exhibited significant correlations with soil pH. The combination of MBT'_{6me} and MBT'_{6me} has the potential to be a proxy for the identification of climatic types. The low MBT'_{5me} (<0.65) and high MBT'_{6me} (>0.55) are diagnostic for the soils developed under cold humid climate.

Acknowledgements *We thank Jia Juan from the Institute of Botany, Chinese Academy of Sciences, for providing some soil samples. This work was supported by the National Natural Science Foundation of China (Grant Nos. 41602189 & 41330103) and the Cradle Plan of China University of Geosciences (Grant No. CUGL170403).*

References

Anderson V J, Shanahan T M, Saylor J E, Horton B K, Mora A R. 2014. Sources of local and regional variability in the MBT′/CBT paleotemperature proxy: Insights from a modern elevation transect across the Eastern Cordillera of Colombia. Org Geochem, 69: 42–51

Bai Y, Fang X, Jia G, Sun J, Wen R, Ye Y. 2015. Different altitude effect of leaf wax *n*-alkane δD values in surface soils along two vapor transport pathways, southeastern Tibetan Plateau. Geochim Cosmochim Acta, 170: 94–107

Bershaw J, Garzione C N, Higgins P, MacFadden B J, Anaya F, Alvarenga H. 2010. Spatial-temporal changes in Andean plateau climate and elevation from stable isotopes of mammal teeth. Earth Planet Sci Lett, 289: 530–538

Besseling M A, Hopmans E C, Sinninghe Damsté J S, Villanueva L. 2017. Benthic Archaea as potential sources of tetraether membrane lipids in sediments across an oxygen minimum zone. Biogeosci Discuss, https://doi.org/10.5194/bg-2017-289

Blaga C I, Reichart G J, Heiri O, Sinninghe Damsté J S. 2008. Tetraether membrane lipid distributions in water-column particulate matter and sediments: A study of 47 European lakes along a north-south transect. J Paleolimnol, 41: 523–540

Blaga C I, Reichart G J, Vissers E W, Lotter A F, Anselmetti F S, Sinninghe Damsté J S. 2011. Seasonal changes in glycerol dialkyl glycerol tetraether concentrations and fluxes in a perialpine lake: Implications for the use of the TEX86 and BIT proxies. Geochim Cosmochim Acta, 75: 6416–6428

Blyth A J, Schouten S. 2013. Calibrating the glycerol dialkyl glycerol tetraether temperature signal in speleothems. Geochim Cosmochim Acta, 109: 312–328

Blyth A J, Jex C N, Baker A, Khan S J, Schouten S. 2014. Contrasting distributions of glycerol dialkyl glycerol tetraethers (GDGTs) in speleothems and associated soils. Org Geochem, 69: 1–10

Cao P, Zhang L M, Shen J P, Zheng Y M, Di H J, He J Z. 2012. Distribution and diversity of archaeal communities in selected Chinese soils. Fems Microbiol Ecol, 80: 146–158

Coffinet S, Huguet A, Williamson D, Fosse C, Derenne S. 2014. Potential of GDGTs as a temperature proxy along an altitudinal transect at Mount Rungwe (Tanzania). Org Geochem, 68: 82–89

Dang X Y, Xue J T, Yang H, Xie S C. 2016a. Environmental impacts on the distribution of microbial tetraether lipids in Chinese lakes with contrasting pH: Implications for lacustrine paleoenvironmental reconstructions. Sci China Earth Sci, 59: 939–950

Dang X, Yang H, Naafs B D A, Pancost R D, Xie S. 2016b. Evidence of moisture control on the methylation of branched glycerol dialkyl glycerol tetraethers in semi-arid and arid soils. Geochim Cosmochim Acta, 189: 24–36

De Jonge C, Hopmans E C, Stadnitskaia A, Rijpstra W I C, Hofland R, Tegelaar E, Sinninghe Damsté J S. 2013. Identification of novel penta- and hexamethylated branched glycerol dialkyl glycerol tetraethers in peat using HPLC-MS^2, GC-MS and GC-SMB-MS. Org Geochem, 54: 78–82

De Jonge C, Hopmans E C, Zell C I, Kim J H, Schouten S, Sinninghe Damsté J S. 2014a. Occurrence and abundance of 6-methyl branched glycerol dialkyl glycerol tetraethers in soils: Implications for palaeoclimate reconstruction. Geochim Cosmochim Acta, 141: 97–112

De Jonge C, Stadnitskaia A, Hopmans E C, Cherkashov G, Fedotov A, Sinninghe Damsté J S. 2014b. *In situ* produced branched glycerol dialkyl glycerol tetraethers in suspended particulate matter from the Yenisei River, Eastern Siberia. Geochim Cosmochim Acta, 125: 476–491

Deng L, Jia G, Jin C, Li S. 2016. Warm season bias of branched GDGT temperature estimates causes underestimation of altitudinal lapse rate. Org Geochem, 96: 11–17

Deng T, Wang S Q, Xie G P, Li Q, Hou S K, Sun B Y. 2011. A mammalian fossil from the Dingqing Formation in the Lunpola Basin, northern Tibet, and its relevance to age and paleo-altimetry. Chin Sci Bull, 57: 261–269

Ding S, Xu Y, Wang Y, He Y, Hou J, Chen L, He J S. 2015. Distribution of branched glycerol dialkyl glycerol tetraethers in surface soils of the Qinghai-Tibetan Plateau: Implications of brGDGTs-based proxies in cold and dry regions. Biogeosciences, 12: 3141–3151

Elling F J, Könneke M, Nicol G W, Stieglmeier M, Bayer B, Spieck E, de la Torre J R, Becker K W, Thomm M, Prosser J I, Herndl G J, Schleper C, Hinrichs K U. 2017. Chemotaxonomic characterisation of the thaumarchaeal lipidome. Environ Microbiol, 19: 2681–2700

Ernst N, Peterse F, Breitenbach S F M, Syiemlieh H J, Eglinton T I. 2013. Biomarkers record environmental changes along an altitudinal transect in the wettest place on Earth. Org Geochem, 60: 93–99

Ghosh P, Garzione C N, Eiler J M. 2006. Rapid uplift of the altiplano revealed through ^{13}C-^{18}O bonds in paleosol carbonates. Science, 311: 511–515

Hough B G, Fan M, Passey B H. 2014. Calibration of the clumped isotope geothermometer in soil carbonate in Wyoming and Nebraska, USA: Implications for paleoelevation and paleoclimate reconstruction. Earth Planet Sci Lett, 391: 110–120

Huguet C, Hopmans E C, Febo-Ayala W, Thompson D H, Sinninghe Damsté J S, Schouten S. 2006. An improved method to determine the absolute abundance of glycerol dibiphytanyl glycerol tetraether lipids. Org Geochem, 37: 1036–1041

Jia G, Wei K, Chen F, Peng P. 2008. Soil *n*-alkane δD vs. altitude gradients along Mount Gongga, China. Geochim Cosmochim Acta, 72: 5165–5174

Kim J H, Schouten S, Hopmans E C, Donner B, Sinninghe Damsté J S. 2008. Global sediment core-top calibration of the TEX_{86} paleothermometer in the ocean. Geochim Cosmochim Acta, 72: 1154–1173

Kim J H, van der Meer J, Schouten S, Helmke P, Willmott V, Sangiorgi F, Koç N, Hopmans E C, Damsté J S S. 2010. New indices and calibrations derived from the distribution of crenarchaeal isoprenoid tetraether lipids: Implications for past sea surface temperature reconstructions. Geochim Cosmochim Acta, 74: 4639–4654

Lehtovirta L E, Prosser J I, Nicol G W. 2009. Soil pH regulates the abundance and diversity of Group 1.1c Crenarchaeota. Fems Microbiol Ecol, 70: 367–376

Lehtovirta L E, Sayavedra-Soto L A, Gallois N, Schouten S, Stein L Y, Prosser J I, Nicol G W. 2016. Identifying potential mechanisms enabling acidophily in the ammonia-oxidizing archaeon "*Candidatus Nitrosotalea devanaterra*". Appl Environ Microbiol, 82: 2608–2619

Lei Y, Yang H, Dang X, Zhao S, Xie S. 2016. Absence of a significant bias towards summer temperature in branched tetraether-based paleothermometer at two soil sites with contrasting temperature seasonality. Org Geochem, 94: 83–94

Li F, Zheng F, Wang Y, Liu W, Zhang C L. 2017. Thermoplasmatales and methanogens: Potential association with the Crenarchaeol oroduction in Chinese soils. Front Microbiol, 8: https://doi.org/10.3389/fmicb.2017.01200

Liu W, Wang H, Zhang C L, Liu Z, He Y. 2013. Distribution of glycerol dialkyl glycerol tetraether lipids along an altitudinal transect on Mt. Xiangpi, NE Qinghai-Tibetan Plateau, China. Org Geochem, 57: 76–83

Oppermann B I, Michaelis W, Blumenberg M, Frerichs J, Schulz H M, Schippers A, Beaubien S E, Krüger M. 2010. Soil microbial community changes as a result of long-term exposure to a natural CO_2 vent. Geochim Cosmochim Acta, 74: 2697–2716

Peterse F, van der Meer M T J, Schouten S, Jia G, Ossebaar J, Blokker J, Sinninghe Damsté J S. 2009. Assessment of soil *n*-alkane δD and branched tetraether membrane lipid distributions as tools for paleoelevation reconstruction. Biogeosciences, 6: 2799–2807

Peterse F, van der Meer J, Schouten S, Weijers J W H, Fierer N, Jackson R B, Kim J H, Sinninghe Damsté J S. 2012. Revised calibration of the MBT-CBT paleotemperature proxy based on branched tetraether membrane lipids in surface soils. Geochim Cosmochim Acta, 96: 215–229

Pitcher A, Rychlik N, Hopmans E C, Spieck E, Rijpstra W I C, Ossebaar J, Schouten S, Wagner M, Sinninghe Damsté J S. 2010. Crenarchaeol dominates the membrane lipids of Candidatus Nitrososphaera gargensis, a thermophilic Group I.1b Archaeon. Isme J, 4: 542–552

Powers L A, Werne J P, Johnson T C, Hopmans E C, Sinninghe Damsté J S, Schouten S. 2004. Crenarchaeotal membrane lipids in lake sediments: A new paleotemperature proxy for continental paleoclimate reconstruction? Geology, 32: 613

Powers L, Werne J P, Vanderwoude A J, Sinninghe Damsté J S, Hopmans E C, Schouten S. 2010. Applicability and calibration of the TEX_{86} paleothermometer in lakes. Org Geochem, 41: 404–413

Schouten S, Hopmans E C, Schefuß E, Sinninghe Damsté J S. 2002. Distributional variations in marine crenarchaeotal membrane lipids: A new tool for reconstructing ancient sea water temperatures? Earth Planet Sci Lett, 204: 265–274

Schouten S, Hopmans E C, Sinninghe Damsté J S. 2013. The organic geochemistry of glycerol dialkyl glycerol tetraether lipids: A review. Org Geochem, 54: 19–61

Sinninghe Damsté J S, Ossebaar J, Schouten S, Verschuren D. 2008. Altitudinal shifts in the branched tetraether lipid distribution in soil from Mt. Kilimanjaro (Tanzania): Implications for the MBT/CBT continental palaeothermometer. Org Geochem, 39: 1072–1076

Sinninghe Damsté J S, Rijpstra W I C, Hopmans E C, Jung M Y, Kim J G, Rhee S K, Stieglmeier M, Schleper C. 2012. Intact polar and core glycerol dibiphytanyl glycerol tetraether lipids of group I.1a and I.1b thaumarchaeota in soil. Appl Environ Microbiol, 78: 6866–6874

Sun J, Xu Q, Liu W, Zhang Z, Xue L, Zhao P. 2014. Palynological evidence for the latest Oligocene-early Miocene paleoelevation estimate in the Lunpola Basin, central Tibet. Palaeogeogr Palaeoclimatol Palaeoecol, 399: 21–30

Wang H, Liu W, Zhang C L. 2014. Dependence of the cyclization of branched tetraethers (CBT) on soil moisture in the Chinese Loess Plateau and the adjacent areas: Implications for palaeorainfall reconstructions. Biogeosci Discuss, 11: 10015–10043

Wang H, Liu W, Lu H. 2016. Appraisal of branched glycerol dialkyl glycerol tetraether-based indices for North China. Org Geochem, 98: 118–130

Wang M D, Liang J, Hou J Z, Hu L. 2016. Distribution of GDGTs in lake surface sediments on the Tibetan Plateau and its influencing factors. Sci China Earth Sci, 59: 961–974

Weijers J W H, Schouten S, Hopmans E C, Geenevasen J A J, David O R P, Coleman J M, Pancost R D, Sinninghe Damsté J S. 2006. Membrane lipids of mesophilic anaerobic bacteria thriving in peats have typical archaeal traits. Environ Microbiol, 8: 648–657

Weijers J W H, Schouten S, van den Donker J C, Hopmans E C, Sinninghe Damsté J S. 2007. Environmental controls on bacterial tetraether membrane lipid distribution in soils. Geochim Cosmochim Acta, 71: 703–713

Weijers J W H, Wiesenberg G L B, Bol R, Hopmans E C, Pancost R D. 2010. Carbon isotopic composition of branched tetraether membrane lipids in soils suggest a rapid turnover and a heterotrophic life style of their source organism(s). Biogeosciences, 7: 2959–2973

Yang H, Ding W, He G, Xie S. 2010. Archaeal and bacterial tetraether membrane lipids in soils of varied altitudes in Mt. Jianfengling in South China. J Earth Sci, 21 (Suppl): 277–280

Yang H, Pancost R D, Dang X, Zhou X, Evershed R P, Xiao G, Tang C, Gao L, Guo Z, Xie S. 2014a. Correlations between microbial tetraether lipids and environmental variables in Chinese soils: Optimizing the paleo-reconstructions in semi-arid and arid regions. Geochim Cosmochim Acta, 126: 49–69

Yang H, Xiao W, Jia C, Xie S. 2014b. Paleoaltimetry proxies based on bacterial branched tetraether membrane lipids in soils. Front Earth Sci, 9: 13–25

Yang H, Lü X, Ding W, Lei Y, Dang X, Xie S. 2015. The 6-methyl branched tetraethers significantly affect the performance of the methylation index (MBT′) in soils from an altitudinal transect at Mount Shennongjia. Org Geochem, 82: 42–53

Yang H, Pancost R D, Jia C, Xie S. 2016. The response of archaeal tetraether membrane lipids in surface soils to temperature: A potential paleothermometer in paleosols. Geomicrobiol J, 33: 98–109

Zang J, Lei Y Y, Yang H. 2018. Distribution of archaeal and bacterial tetraether lipids in the surface soil of Turpan: Implications for the use of tetraether-based proxies in hot and dry regions. Front Earth Sci, unpublished

Zheng F F, Zhang C L, Chen Y F, Li F Y, Ma C L, Pu Y, Zhu Y Q, Wang Y L, Liu W G. 2016. Branched tetraether lipids in Chinese soils: Evaluating the fidelity of MBT/CBT proxies as paleoenvironmental proxies. Sci China Earth Sci, 59: 1353–1367

Zhou H, Hu J, Spiro B, Peng P, Tang J. 2014. Glycerol dialkyl glycerol tetraethers in surficial coastal and open marine sediments around China: Indicators of sea surface temperature and effects of their sources. Palaeogeogr Palaeoclimatol Palaeoecol, 395: 114–121

Zhuang G, Brandon M T, Pagani M, Krishnan S. 2014. Leaf wax stable isotopes from Northern Tibetan Plateau: Implications for uplift and climate since 15 Ma. Earth Planet Sci Lett, 390: 186–198

Zhuang G, Pagani M, Chamberlin C, Strong D, Vandergoes M. 2015. Altitudinal shift in stable hydrogen isotopes and microbial tetraether distribution in soils from the Southern Alps, NZ: Implications for paleoclimatology and paleoaltimetry. Org Geochem, 79: 56–64

(Responsible editor: Huayu LU)